Phonon partial densities of states and entropies of Fe and Cr in bcc Fe-Cr from inelastic neutron scattering

Matthew S. Lucas, M. Kresch, R. Stevens, and B. Fultz
California Institute of Technology, W. M. Keck Laboratory, P.O. Box 138-78, Pasadena, California 91125, USA
(Received 8 October 2007; revised manuscript received 27 March 2008; published 9 May 2008)

Inelastic neutron-scattering spectra were measured on disordered solid solutions of body-centered cubic Fe-Cr alloys of different compositions. These data were reduced from time-of-flight histograms to energy spectra that resemble the phonon density of states (DOS) but were distorted by differences in efficiencies of the atom species for phonon scattering. Cluster expansion formalisms were developed to both correct this neutron-weighting problem and isolate phonon partial DOS curves of Fe and Cr atoms. An asymmetry in the phonon entropy of mixing was identified and attributed to the larger number of low-energy modes associated with like and unlike pairs in the first and second nearest-neighbor shells of Cr atoms compared to Fe atoms. The effect of the phonon entropy on chemical unmixing is found to both lower the critical temperature and shift the critical composition substantially.

DOI: 10.1103/PhysRevB.77.184303 PACS number(s): 63.50.−x, 78.70.Nx

I. INTRODUCTION

A disordered solid solution, where two or more species of atoms are distributed at random on the sites of a crystal lattice, is often the thermodynamically stable state over a range of compositions, especially for metallic alloys. Owing to their entropy of configurations S_{cf}, disordered solid solutions are not expected to be thermodynamically favorable at arbitrarily low temperatures compared to, for example, mixtures of ordered compounds or combinations of chemically unmixed structures. At higher temperatures, solid solutions are expected to be stable over wider ranges of composition owing to S_{cf}. The stability of solid solutions can be significantly altered, however, by compositional variations of the phonon entropy S_{ph}. In several alloys, the phonon entropy is comparable to the configurational entropy[1–5] and is sometimes even larger.[6] The role of S_{ph} on the relative stabilities of alloy phases is an active area of research.[7–14] The electronic origin of phonon dynamics has been of interest over many years.[15–18] Systematics of how S_{ph} depends on atomic size and bond lengths are also of interest.[2,3,19–21,34] Any explanation, however, must account for how the spectral distribution of the phonon density of states (DOS) depends on the atom configurations on the lattice. The present work provides a systematic way to interpret the phonon DOS in terms of the local configurations of atoms in disordered solid solutions.

For phonon thermodynamics, the DOS is a central quantity. Knowing the numbers of phonons in each small energy interval is sufficient to construct a partition function for phonons. A powerful method for measuring the DOS by thermal neutron scattering is with a time-of-flight chopper spectrometer. The intensity of energy transfers from the neutron to the sample can be interpreted as the spectrum of phonon creations and annihilations and often the single-phonon excitation spectrum can be obtained. For alloys, a challenge for this method is that different elements have different efficiencies for phonon scattering, which are proportional to the ratio of their neutron scattering cross-section σ_{sc} to their atomic mass m. The displacements of different atoms in different phonons usually have different amplitudes so different phonons may be over- or under-represented in a DOS directly obtained from experimental measurements. The distortion of the phonon DOS is termed the "neutron-weighting" problem,[4,22] and its solution is termed a neutron-weight correction.

Solving the neutron-weighting problem is tantamount to obtaining the phonon partial density of states (PDOS) curves for each element in the alloy (the PDOS curves weight the amplitudes of displacement of each element for each phonon). When there is a translational periodicity, as for chemically ordered alloys, inverting a Born-von Kármán lattice dynamics model can provide PDOS curves and neutron-weight corrections for experimental data.[23–25] A less explored approach, which is based on cluster expansion methods, offers opportunities for chemically disordered alloys. Usually, this method is used to determine disordered properties from ordered properties.[26] It has been used in approximate corrections of the phonon entropy in Cu-Au[22] and for a nuclear resonant inelastic x-ray scattering (NRIXS) experiment.[4] Recently, the formalism of the cluster expansion was extended to the DOS curves themselves.[27,28]

Both pure Fe and pure Cr have the body-centered cubic (bcc) structure at low temperatures and bcc solid solutions are stable in the Fe-Cr alloy system at all compositions and modest temperatures. At low temperatures, Fe-Cr solid solutions exhibit chemical unmixing over a broad range of compositions around the equiatomic compositions. Much experimental work on the Fe-Cr system has addressed this "spinodal decomposition," owing to its correlation with the brittleness of ferritic stainless steels.[29,30] The thermodynamics of Fe-Cr solid solutions is an important starting place for understanding the metals physics of this unmixing. It is now known, for example, that the critical temperature is lowered by the relatively large S_{ph} of the solid solution.[4] Fortunately, the high-temperature disordered state of Fe-Cr is not difficult to preserve at low temperatures by rapid cooling and it is possible to prepare alloys of Fe-Cr of all compositions as bcc solid solutions with similar lattice parameters.

II. EXPERIMENT

Alloys of stoichiometric $Fe_{1-x_{Cr}}Cr_{x_{Cr}}$ for $x_{Cr}=\{1,0.99,0.97,0.90,0.80,0.70,0.47,0.30,0\}$ were prepared from shots of 99.99% Fe and 99.995% Cr by arc melting under an argon atmosphere. There was a negligible mass loss and little visible surface oxidation after melting so the compositions are expected to be accurate to 0.1%. The samples of composition $x_{Cr}\geq 0.70$ were then crushed to a thickness corresponding to a neutron-scattering probability of 10%. The samples were sealed in quartz tubes under an argon atmosphere and annealed at 1100 °C for several hours, which was followed by a quench into an iced brine to ensure that the samples were random solid solutions. Samples with higher Fe concentration were ductile enough to be cold rolled to thicknesses corresponding to a neutron-scattering probability of 10%. These samples were sealed in quartz tubes under an argon atmosphere and annealed for several days at 1100 °C. The longer anneal time for the rolled samples reduced the crystallographic orientation induced by the rolling.

X-ray diffraction patterns were acquired for all samples both before and after the anneal. The patterns indicated that all samples had the bcc structure. There was no measurable evidence of the sigma phase or of oxidation. Mössbauer spectroscopy was performed on all of the samples after the anneal. The spectra showed no indication of chemical unmixing.

Time-of-flight inelastic neutron-scattering data were acquired using the low resolution medium energy chopper spectrometer (LRMECS) instrument at the Intense Pulsed Neutron Source at Argonne National Laboratory. Samples were mounted in thin-wall aluminum cans of dimensions 7×10 cm^2. The incident beam of monochromatic neutrons had an energy of approximately 60 meV. The flat sample packages were tilted at a 45 degree angle off the direction of the incident beam to minimize self shielding. All spectra were measured at room temperature. Background data were acquired from the empty aluminum cans under the same conditions.

III. DATA ANALYSIS AND RESULTS

Our data include both coherent and incoherent scattering from samples that are both polyatomic and polycrystalline. The total scattering cross-section is given by the sum of the coherent and incoherent scattering. The incoherent neutron-scattering cross-section for nuclear scattering by a single crystal monatomic system is

$$\left(\frac{d\sigma}{d\Omega dE'}\right)^{\text{inc}}=\frac{k'}{k}\frac{N\sigma_{\text{inc}}}{2\pi\hbar}e^{-2W}\int e^{\langle UV\rangle}e^{(-i\omega t)}dt, \tag{1}$$

where $U=-i\mathbf{Q}\cdot\mathbf{u}(0)$, $V=i\mathbf{Q}\cdot\mathbf{u}(t)$. The variables σ_{inc}, $\mathbf{u}(t)$, W, N, $\mathbf{k}$, $\mathbf{k}'$, $\mathbf{Q}$, and $E=\hbar\omega$ are the incoherent cross-section, instantaneous atomic position, Debye-Waller factor, number of atoms in the system, initial and final neutron wave vectors, phonon wave vector (wave vector transfer), and phonon energy, respectively. Our first approximation is that all the measured scattering is incoherent. Despite the fact that both Fe and Cr are strong coherent scatterers (with $\sigma_{\text{inc,Fe}}=0.40$, $\sigma_{\text{coh,Fe}}=11.22$, $\sigma_{\text{inc,Cr}}=1.66$, and $\sigma_{\text{inc,Cr}}=1.83$ barns), the incoherent approximation (IA) is acceptable when the inelastic scattering is measured over a broad range of $\mathbf{Q}$ and E (Ref. 31) and the structure in $\mathbf{Q}$ is averaged away.

The incoherent scattering cross-section contains both elastic and inelastic contributions. The elastic scattering can be removed from the raw data so we concern ourselves only with the inelastic scattering. The inelastic scattering is a sum of the single and multiphonon scattering

$$\left(\frac{d\sigma}{d\Omega dE'}\right)^{\text{inc}}_{\text{inelastic}}=\sum_{n=1}^{\infty}\left(\frac{d\sigma}{d\Omega dE'}\right)^{\text{inc}}_{n\text{-phonon}}, \tag{2}$$

where n denotes the number of phonons created or annihilated in the scattering event,

$$\left(\frac{d\sigma}{d\Omega dE'}\right)^{\text{inc}}_{n\text{-phonon}}=\frac{k'}{k}\frac{N\sigma_{\text{inc}}}{4\pi\hbar}\frac{e^{-2W}}{n!}\left(\frac{3\hbar}{2m}\right)^{n}[P(\omega)]^{n\text{-convolution}}, \tag{3}$$

where m is the mass of the scatterer, and

$$P(\omega)=\frac{\langle(\mathbf{Q}\cdot\mathbf{e}_s)^2\rangle_{\omega}}{\omega}g(\hbar\omega)\langle n_{\omega}+1\rangle+\frac{\langle(\mathbf{Q}\cdot\mathbf{e}_s)^2\rangle_{-\omega}}{-\omega}g(-\hbar\omega)\langle n_{-\omega}\rangle. \tag{4}$$

The index s specifies a single vibrational mode and the notation $[f]^{n\text{-convolution}}$ specifies the sequential convolution of n instances of the function f. The quantity $\langle(\mathbf{Q}\cdot\mathbf{e}_s)^2\rangle_{\omega}$ is the value of $(\mathbf{Q}\cdot\mathbf{e}_s)^2$ averaged over all modes of frequency ω. This is equivalent to averaging over all directions and shows that the incoherent scattering cross-section is the same for single crystal and polycrystalline samples. The incoherent one-phonon scattering for a monatomic polycrystalline sample is then

$$\left(\frac{d\sigma}{d\Omega dE'}\right)^{\text{inc}}_{1-\text{phonon}}=\frac{k'}{k}\frac{\sigma_{\text{inc}}}{4\pi}\frac{N}{4m}Q^2e^{-2W}\frac{g(\hbar\omega)}{\omega}\left[\coth\left(\frac{1}{2}\hbar\omega\beta\right)\pm 1\right], \tag{5}$$

where $\beta=1/(k_BT)$. The + denotes phonon creation and the − phonon annihilation.

For a polyatomic sample, we invoke a virtual crystal approximation (VCA), which assumes a single mass and scattering factor for an average atom:

$$g^{\text{nw}}(E,\vec{\sigma})e^{(-2\langle W\rangle_d)}\left\langle\frac{\sigma_{\text{sc}}}{m}\right\rangle_d=\sum_d g(E,\vec{\sigma},d)e^{-2W_d}\frac{\sigma_{\text{sc},d}}{m_d}. \tag{6}$$

Here, $g^{\text{nw}}(E,\vec{\sigma})$ is the DOS that results from the VCA and is termed the neutron-weighted density of states (NWDOS), which is a function of the configuration of atoms on the lattice $\vec{\sigma}$. The phonon partial density of states (PDOS) of atom d for a given local chemical arrangement $\vec{\sigma}_l$ is given by $g(E,\vec{\sigma}_l,d)$. The $\langle\cdots\rangle_d$ denotes an average over all atoms. The $g^{\text{nw}}(E,\vec{\sigma})$ are obtained from the raw data by the following procedure.

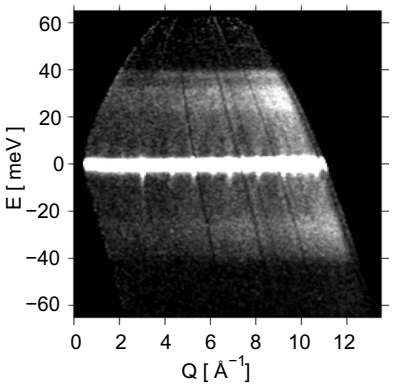

FIG. 1. Measured $I(Q,E)$ for pure Cr, where E is the neutron energy transfer to the sample. White indicate areas of higher intensity, with the large elastic peak evident at 0 meV. Coherent scattering can be seen to emanate from the Bragg peaks.

The raw data expressed in terms of intensity as a function of detector number and time-of-flight, were first corrected for the efficiency of the detectors by using a white beam measurement of pure vanadium (a fully incoherent scatterer). The data were then normalized by using the integrated intensity in the beam monitor. An average of the counts at the longest times-of-flight was taken as an estimate of the time-of-flight independent background, and removed. The data were rebinned into intensity I as a function of angle ϕ from 5 to 145° by 0.6°, and energy E from −65.0 to 65.0 meV by 0.5 meV. The data were again rebinned to give intensity $I(Q,E)$, where Q is the wave vector transfer, which ranged from 0.0 to 13.5 Å^{-1} by 0.0675 Å^{-1}. The spectrum from the empty container, which was scaled by 0.9 to account for the self shielding of the sample, was subtracted from the data. An example of such a corrected $I(Q,E)$ is shown in Fig. 1. The data were cropped below $Q \approx 2.8$ Å^{-1} to minimize contributions from magnetic scattering, which dominates at small Q. After removal of an elastic peak centered about 0 meV, the data approximately below 10 meV were replaced by the function $\mathcal{A}E/[1-\exp(-\beta E)]$ with a normalization constant $\mathcal{A}$, which was determined from the data. The instrument resolution for positive neutron energy transfer is much better than for negative (see Fig. 1) so only the data for $E > 0$ were used for determining $g^{\mathrm{nw}}(E,\vec{\sigma})$.

Finally, under the assumptions of the VCA and the IA, we recover the one- phonon DOS by using the iterative procedure described by Sears *et al.*[32] as modified by Kresch *et al.*[33] This procedure corrects for thermal occupancy, Debye-Waller factor, multiphonon (2-through 5-phonon) and multiple scattering as a function of Q, and then the (neutron-weighted) phonon DOS is the sum over all Q of the corrected data. These NWDOS curves are normalized to one in energy and presented in Fig. 2.

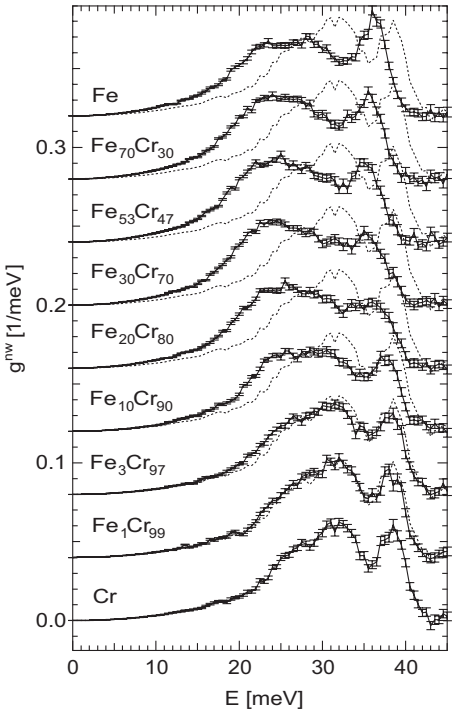

FIG. 2. Measured NWDOS curves for alloys $g^{\mathrm{nw}}(E)$ and $g(E)$ for elements. The dashed lines are the measured Cr DOS for comparison. Curves are offset by integer multiples of 0.04 meV^{-1}.

IV. DISCUSSION

A. Phonon partial DOS

The NWDOS is a linear combination of the PDOS, which is distorted by the differences in the efficiencies of phonon scattering of the different atoms. To calculate thermodynamic quantities, such as the vibrational entropy or phonon contribution to the heat capacity, the undistorted total phonon DOS is required,

$$g(E,\vec{\sigma}) = \sum_d g(E,\vec{\sigma}_l,d)x_d, \tag{7}$$

where x_d is the concentration of atom species d $(0 \le x_d \le 1)$. We assume that $\exp[-2(\langle W\rangle_d - W_d)] \simeq 1$, which is most reliable at low temperatures, so that Eq. (6) becomes

$$g^{\mathrm{nw}}(E,\vec{\sigma}) = \left\langle \frac{\sigma_{\mathrm{sc}}}{m} \right\rangle_d^{-1} \sum_d g(E,\vec{\sigma}_l,d)\frac{\sigma_{\mathrm{sc},d}}{m_d}x_d, \tag{8}$$

where the normalization factor is given by

$$\left\langle \frac{\sigma_{\mathrm{sc}}}{m} \right\rangle_d = \left(\sum_d \frac{\sigma_{\mathrm{sc},d}}{m_d}x_d \right). \tag{9}$$

In our case, phonon scattering from natural Fe is approximately three times stronger than that from natural Cr, or $\sigma_{\mathrm{sc,Fe}}/m_{\mathrm{Fe}} \simeq 3\sigma_{\mathrm{sc,Cr}}/m_{\mathrm{Cr}}$. The data reduction technique described in Sec. III produces a NWDOS, where the Fe PDOS is overweighted by a factor of 3. This distorts the NWDOS from the true DOS if the Fe PDOS significantly differs from the Cr PDOS.

NRIXS is a synchrotron technique used to determine the PDOS of a Mössbauer isotope such as ^{57}Fe (Refs. 35–38). The available Fe PDOS curves from NRIXS[28] can be directly used in a neutron-weight correction for the alloys $Fe_{30}Cr_{70}$, $Fe_{53}Cr_{47}$, and $Fe_{70}Cr_{30}$. The Cr PDOS curves can then be determined using Eq. (8), with the results shown in

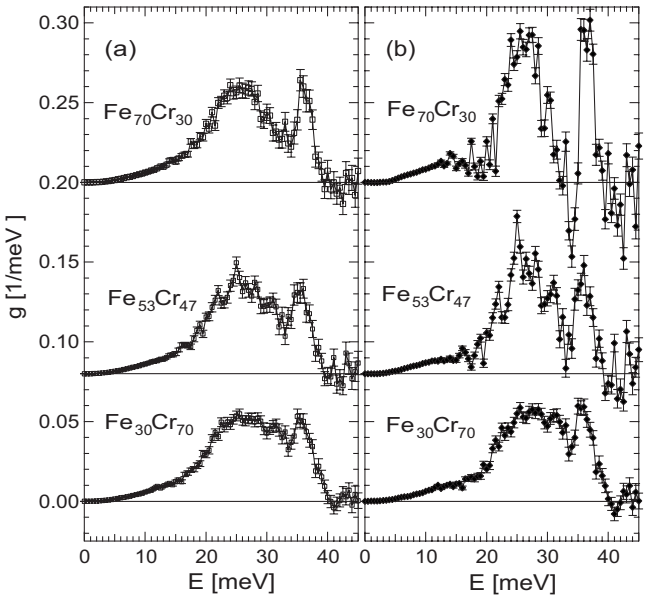

FIG. 3. (a) Neutron-weight-corrected DOS for $Fe_{30}Cr_{70}$, $Fe_{53}Cr_{47}$, and $Fe_{70}Cr_{30}$ by using Fe PDOS curves from NRIXS.[28] (b) Cr PDOS curves determined from measured NWDOS and Fe PDOS curves from NRIXS. The curves for $Fe_{53}Cr_{47}$ and $Fe_{70}Cr_{30}$ are offset by 0.08 and 0.20 meV^{-1}, respectively.

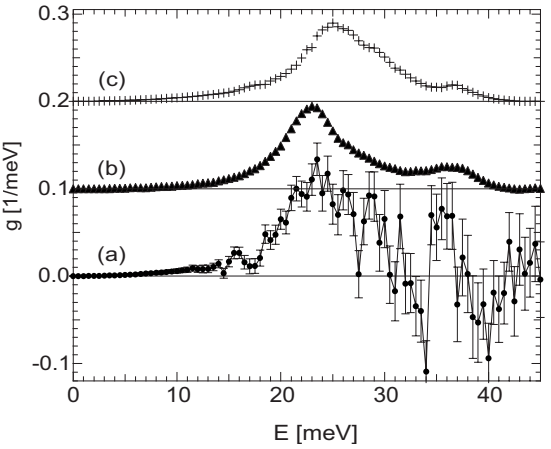

FIG. 4. PDOS of Fe in Fe_3Cr_{97} (a) determined from the results in the present article following the subtraction method given in the text, (b) the results of NRIXS from the literature[39] (offset by 0.1 meV^{-1}), and (c) determined from Mannheim Method with $K_{Cr-Cr}/K_{Fe-Cr}=1.26$ using pure Cr measured at LRMECS (offset by 0.2 meV^{-1}).

Fig. 3. Especially at low Fe concentrations, knowledge of the Fe PDOS from NRIXS is useful for determining the Cr PDOS. At higher Fe concentrations, the scattering from the Cr atoms is overwhelmed by that of Fe atoms and a larger Fe PDOS must be removed from the measured NWDOS to determine the Cr PDOS. This inherently poor signal-to-noise for the Cr PDOS is evident in Fig. 3 for the alloy $Fe_{70}Cr_{30}$.

The following sections describe a different method for determining the Cr and Fe PDOS curves. This method utilizes a cluster expansion technique to extract chemical trends from the NWDOS curves. For inputs, this method requires two PDOS curves from dilute Fe-Cr and Cr-Fe alloys. Section IVB shows how these two "impurity" PDOS curves can be derived from the data set in Fig. 2 with two different methods. Section IV C describes the cluster expansion technique. Only the results of neutron-scattering experiments are used in the subsequent analysis. The available results from NRIXS[28,39] provide a verification of the method.

B. PDOS in the dilute limit

This section presents two methods for obtaining the PDOS of an impurity atom in an otherwise pure host. The first method uses only the measured NWDOS curves of Fig. 2 but the statistical quality of the present data requires the use of the second method. Both methods rely on the assumption that the PDOS of the host atoms is unaltered by the impurity atoms. For V with impurities of Cr, this assumption has been shown to be good, owing to the similarities of the Fermi surface of V and V-Cr,[6,18] and for the same reason, we expect this to be valid for Fe-Cr. The PDOS measured by NRIXS of Fe_3Cr_{97} provides a check of this assumption for Fe-Cr.

Comparing the measured DOS of the pure element to the measured NWDOS of a sample with small amounts of impurity atoms can provide the PDOS of the impurity atom by using Eq. (8). Figure 4(a) shows the impurity PDOS of 3% Fe in Cr, which is determined with this method by weighted subtraction of the lower curves of Fig. 2. Although the error bars are quite large, it is apparent that the agreement with the result of NRIXS[39] is reasonable. Within the quality of our experimental results, a decomposition into a host, plus impurity PDOS curves, is successful for Fe-Cr dilute alloys. Determination of the Cr PDOS curves from this method suffers from much larger error bars due to the lower scattering efficiency of Cr atoms. Another method for acquiring the PDOS of impurity Cr atoms is required.

The lattice dynamics of crystals with dilute impurities was developed by Mannheim,[40,41] with Green's function techniques for interatomic force constants, described by a single longitudinal stiffness. The assumption is made that the introduction of the impurity perturbs only the first nearest- neighbor (1NN) bonds to the impurity atom. The only information required for this theory are the DOS of the pure host, the mass ratio of the host to the impurity atoms m_h/m_d, and the ratio of the host-host force constant to the impurity-host force constant $K_{h\text{-}h}/K_{d\text{-}h}$. The force constants of Fe-Cr alloys have been previously determined by inelastic neutron scattering.[42] The ratio $K_{h\text{-}h}/K_{d\text{-}h}$ can be approximated by the ratio of the 1NN longitudinal force constants of the pure host with the 50–50 alloy. For Fe in Cr, this ratio is 1.26, which is similar to the previously reported value of 1.25.[43] The value obtained for Cr in Fe is 1.01, which has been used in determining the impurity Cr PDOS in Fe. The impurity PDOS of Fe, which is determined from the Mannheim method by using the pure Cr DOS measured with LRMECS, is shown in Fig. 4(c). The results of the Mannheim method for the PDOS curves of both Fe and Cr in the dilute limit are used in the analysis that follows below.

C. Cluster expansion method

A cluster expansion is a systematic method for expressing a thermodynamic quantity $J(\vec{\sigma})$ in terms of the chemical arrangement $\vec{\sigma}$ on a particular lattice.[44–50] A set of atomic correlation functions $\{\xi_n\}$ is unique to each chemical arrangement $\vec{\sigma}$, whereas the interaction parameters $\mathcal{J}_n$ are constant for alloys with the same lattice and specific volume.[26,2] Each interaction *parameter* provides a measure of the thermodynamic contribution from each type of cluster. For example, the interaction phonon entropies provide a measure of the phonon entropy associated with each of the terms in the cluster expansion. Interaction *functions* $\mathcal{J}_n(E)$, where E is the energy of the quantum state associated with the particular thermodynamic quantity, provide a more detailed picture of the contributions from each cluster type. In the case of the phonon entropy, the associated function is the DOS or PDOS.[28] The interaction phonon density of states (IDOS) and interaction phonon partial density of states (IPDOS) functions provide detailed information on how the chemical arrangement changes the DOS and PDOS curves, respectively. Physically, the forces in a system could have a long range, but if the changes in the local chemical arrangement control them, only short-range clusters are necessary (i.e., a useful cluster size may or may not represent the range of the forces).

Two types of cluster expansions prove necessary for studies of alloys by neutron scattering: one for local thermodynamic properties and the other for overall thermodynamics. The PDOS is an average over a particular atom species, the DOS is an average over all atom species, and the DOS is a weighted sum of the PDOS functions [Eq. (7)]. Typically, a cluster expansion is performed over all atom species in what has been termed the general cluster expansion (GCE). To account for the PDOS, a cluster expansion must be performed on a particular atom species by using a local order cluster expansion (LOCE).[51] Both types of cluster expansions are similar in their mathematics but different in their interpretations. A precise definition of these two types of expansions is given in Appendix A.

The first step in performing a cluster expansion is to rescale the NWDOS curves by the phonon cutoff energy $E^c(\vec{\sigma})$, which is defined as

$$g(E,\vec{\sigma}) = 0, E > E^c(\vec{\sigma}). \tag{10}$$

The rescaled energy, $\mathcal{E}$, is given by

$$\mathcal{E} = \mathcal{E}(\vec{\sigma}) = \frac{E}{E^c(\vec{\sigma})}, \tag{11}$$

where $0 \leq \mathcal{E} \leq 1$. This step helps to separate the effects of changes in bond length and bond stiffness from the effects of atom arrangement for which the cluster expansion is designed.

The next step is to determine the neutron-weighted interaction phonon density of states (NWIDOS) functions $\mathcal{G}_n^{\mathrm{nw}}(\mathcal{E})$. The limitations of using random solid solutions for the determination of interaction functions have been previously assessed by using the condition number of the correlation function matrix.[28] Here, we simply note that only a small number of terms can be used when extracting chemical trends from measurements of random solid solutions, owing to the lack of both long-range and short-range order. For this reason, a GCE using four terms, up to the triangle cluster, is utilized for the NWDOS. The relation between the NWDOS curves of a random solid solution of concentration x_{Cr}, $g^{\mathrm{nw}}(\mathcal{E},x_{\mathrm{Cr}})$, and the NWIDOS functions is [following Eq. (B6)]

$$g^{\mathrm{nw}}(\mathcal{E},x_{\mathrm{Cr}})\left\langle \frac{\sigma_{\mathrm{sc}}}{m} \right\rangle_d^{-1} = \sum_{n=0}^{3} \mathcal{G}_n^{\mathrm{nw}}(\mathcal{E})(1-2x_{\mathrm{Cr}})^n. \tag{12}$$

Since there are more measurements than terms used in the expansion, the problem is overspecified and a weighted least-squares fitting must be performed to include all of the measured information into the NWIDOS functions. The NWIDOS functions and impurity PDOS curves can be used to determine the IPDOS functions $\mathcal{G}_n(\mathcal{E},d)$, following the method described in Appendix B.

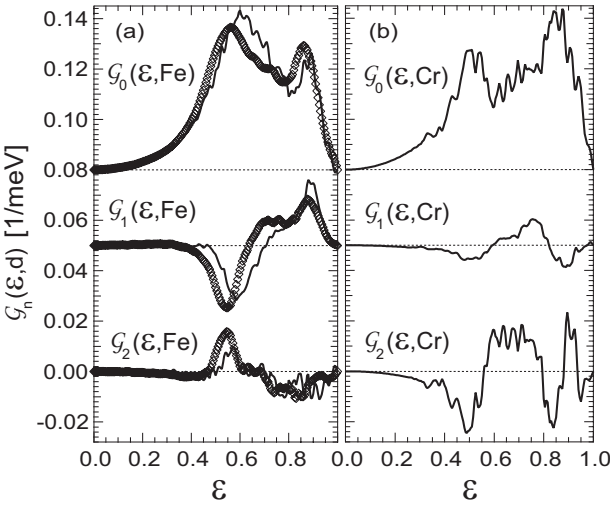

FIG. 5. IPDOS functions of Fe (a) and Cr (b) in Fe-Cr determined from neutron scattering (solid lines) and NRIXS (thick curve). The $n=0$ and $n=1$ terms are offset by 0.08 and 0.05 meV^{-1}, respectively.

D. Interaction phonon partial density of states functions of Fe-Cr

The IPDOS functions of Fe and Cr in Fe-Cr determined from fits to the neutron-scattering data and the impurity PDOS curves determined from the Mannheim method (Sec. IV B) are shown in Fig. 5. For comparison, the PDOS curves of Fe in Fe-Cr alloys determined from NRIXS[28,39] were also used to construct the IPDOS functions of Fe and both sets of $\mathcal{G}_n(\mathcal{E},\mathrm{Fe})$ are compared in Fig. 6. The curves match well, especially in their compositional trends, and agreement is best for the higher Fe concentrations where the neutron-scattering analysis is most reliable.

The effects of local order on the PDOS curves of Fe in Fe-Cr have been previously explained[28] in terms of the $\mathcal{G}_n(\mathcal{E},\mathrm{Fe})$ and the same interpretation is successful for the effects of local order on the PDOS curves of Cr in Fe-Cr. The $n=0$ term is the Cr PDOS of a random solid solution of

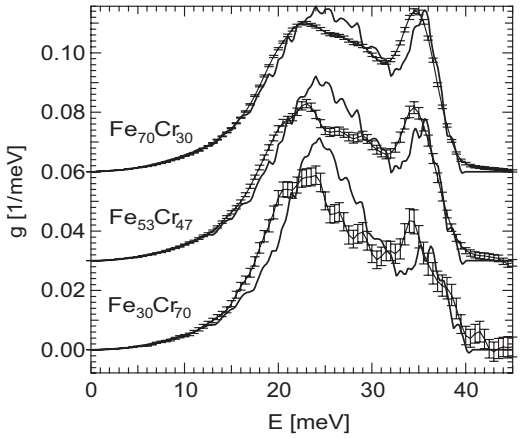

FIG. 6. PDOS curves of Fe determined from neutron scattering (lines) and NRIXS (lines with error bars). Curves are offset by integer multiples 0.03 meV^{-1}.

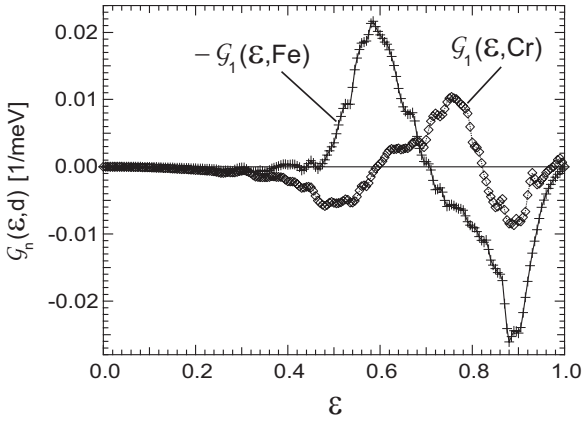

FIG. 7. The dependence on Cr concentration of the Fe and Cr PDOS curves. The minus sign for Fe accounts for the $(-1)^n$ in Eq. (A6).

$Fe_{50}Cr_{50}$. The $n=1$ term gives the effect on the PDOS of having different numbers of Fe and Cr atoms in the 1NN and second nearest-neighbor (2NN) shells of the Cr atom. The triangle term $n=2$ gives the effect of the like or unlike pairs of atoms within the 1NN and 2NN shells of the Cr atom. The function $\mathcal{G}_1(\mathcal{E},\mathrm{Cr})$ is added to $\mathcal{G}_0(\mathcal{E},\mathrm{Cr})$ when the atom in the 1NN and 2NN shell of the Cr atom is Cr and subtracted when it is Fe. Figure 5 shows that the effect of Cr atoms in the 1NN and 2NN shell of the Cr atom is to decrease the number of modes in the ranges of $0 \leq \mathcal{E} \leq 0.59$ and $0.83 \leq \mathcal{E} \leq 1$ while increasing the number of modes in the range $0.59 < \mathcal{E} < 0.83$. The function $\mathcal{G}_2(\mathcal{E},\mathrm{Cr})$ adds to both $\mathcal{G}_0(\mathcal{E},\mathrm{Cr})$ and $\mathcal{G}_1(\mathcal{E},\mathrm{Cr})$ when a pair in the 1NN and 2NN shell of the Cr atom is composed of two of the same atoms. Pairs of like atoms decrease the number of modes in the ranges $0 \leq \mathcal{E} \leq 0.56$, $0.80 \leq \mathcal{E} \leq 0.88$, and $0.94 \leq \mathcal{E} \leq 1$ while increasing the number of modes in the remaining ranges, whereas unlike pairs do the opposite.

Comparing the Fe and Cr IPDOS functions in Fig. 5 provides further information on how a local order alters the phonons in Fe-Cr. To show the effects of Cr concentration on both the Fe and Cr PDOS curves, the function $\mathcal{G}_1(\mathcal{E},\mathrm{Fe})$ must be multiplied by -1, as shown in Fig. 7. With increasing Cr concentration, each of these functions is added to its respective PDOS. In both cases, increasing the Cr concentration decreases the number of low-energy modes in the range $0 \leq \mathcal{E} \leq 0.37$. In the range $0.37 < \mathcal{E} \leq 0.67$, the effects of Cr on the PDOS curves is opposite in sign, with the magnitude of the increase in the Fe modes being much larger than the decrease for Cr. For $\mathcal{E} > 0.82$, the longitudinal modes of both Fe and Cr are reduced (shifted to lower $\mathcal{E}$) by increasing the concentration of Cr. The functions $\mathcal{G}_2(\mathcal{E},\mathrm{Fe})$ and $\mathcal{G}_2(\mathcal{E},\mathrm{Cr})$ have similar features in the range $0 \leq \mathcal{E} \leq 0.70$, indicating similar effects of the pair interaction on the longitudinal modes of both the Fe and Cr PDOS.

The IPDOS functions can be used to construct the PDOS curves of Fe and Cr atoms for our alloys (Fig. 8). These PDOS curves can then be used to construct the neutron-weight-corrected DOS curves by following Eq. (7). The results are shown in Fig. 9. It is evident that the neutron-weight correction stiffens all of the DOS curves. This is expected, as the Fe PDOS curves have more low energy modes than the Cr PDOS curves, especially below $\mathcal{E}=0.7$ but Fe atoms are more efficient scatterers.

E. Phonon entropy

The phonon entropy $S_{\mathrm{ph}}(\vec{\sigma})$ for a specific chemical arrangement $\vec{\sigma}$ is, in the quasiharmonic approximation,[4]

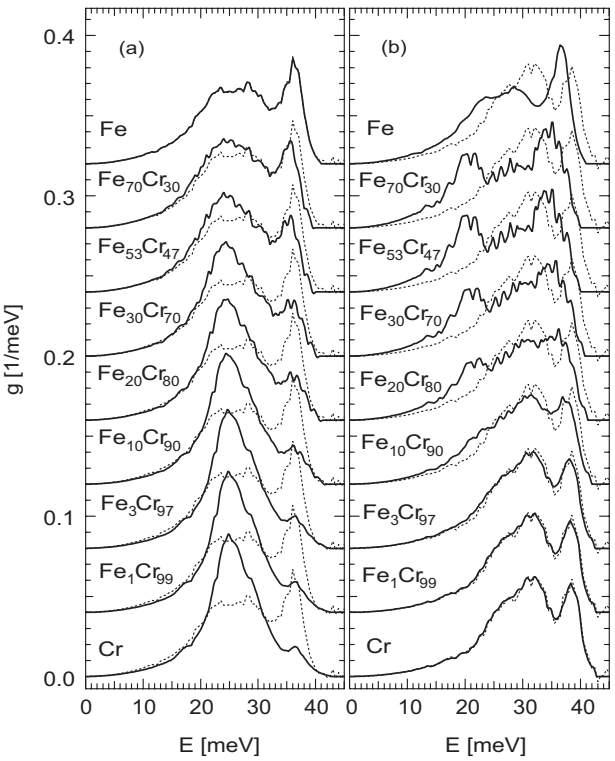

FIG. 8. PDOS curves from the cluster expansion fitting method for the concentrations of the alloys measured: (a) Fe PDOS curves (solid lines) and measured pure Fe DOS (dashed line) and (b) Cr PDOS curves (solid lines) and measured pure Cr DOS (dashed line). Curves are offset by integer multiples 0.04 meV^{-1}.

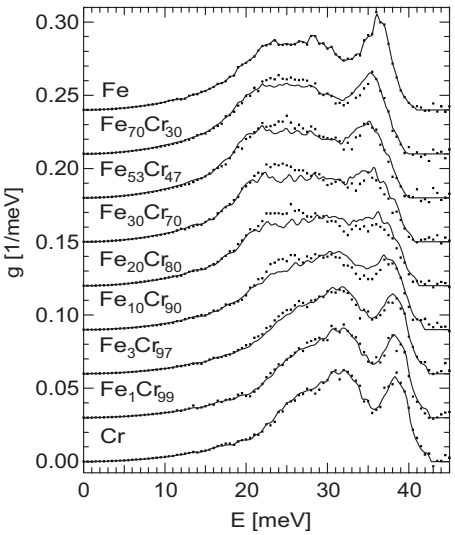

FIG. 9. Neutron-weight-corrected DOS curves from cluster expansion method (solid line) and measured neutron-weighted DOS curves (dots). Curves are offset by integer multiples 0.03 meV^{-1}.

$$S_{\mathrm{ph}}(\vec{\sigma}) = 3k_B \int_0^\infty f^\star(E) g(E,\vec{\sigma}) \mathrm{d}E, \tag{13}$$

with

$$f^\star(E) \equiv [f(E)+1]\ln[f(E)+1] - f(E)\ln[f(E)], \tag{14}$$

where $f(E)$ is the Planck distribution. Both $f(E)$ and $g(E,\vec{\sigma})$ are obtained at the same temperature. The phonon entropy of mixing $\Delta S_{\mathrm{ph}}(\vec{\sigma})$ is given by

$$\Delta S_{\mathrm{ph}}(\vec{\sigma}) = S_{\mathrm{ph}}(\vec{\sigma}) - \sum_d x_d S_{\mathrm{ph}}(x_d = 1), \tag{15}$$

where $S_{\mathrm{ph}}(x_d=1)$ is the phonon entropy of pure element d. The phonon entropies of mixing from the neutron-weighted and weight-corrected DOS curves evaluated at 293 K are shown in Fig. 10. The entropy of mixing of the corrected DOS curves is lower than that for the measured NWDOS curves due to the higher scattering efficiency of the low-energy Fe modes.

The phonon partial entropy $S_{\mathrm{ph}}(\vec{\sigma}_l, d)$ for the specific local chemical arrangement of atom d in a binary system A-B is in the quasiharmonic approximation,

$$S_{\mathrm{ph}}(\vec{\sigma}_l, d) = 3k_B \int_0^\infty f^\star(E) g(E,\vec{\sigma}_l, d) \mathrm{d}E. \tag{16}$$

A LOCE in E must be used to show the effects of each term in the cluster expansion for each atom. This can be done for Fe-Cr since the cutoff energy does not have a strong dependence on the composition. For a random solid solution using a three term LOCE, the only contribution to the phonon partial entropy of mixing $\Delta S_{\mathrm{ph}}(x_d, d)$ comes from the $n=2$ term and is,

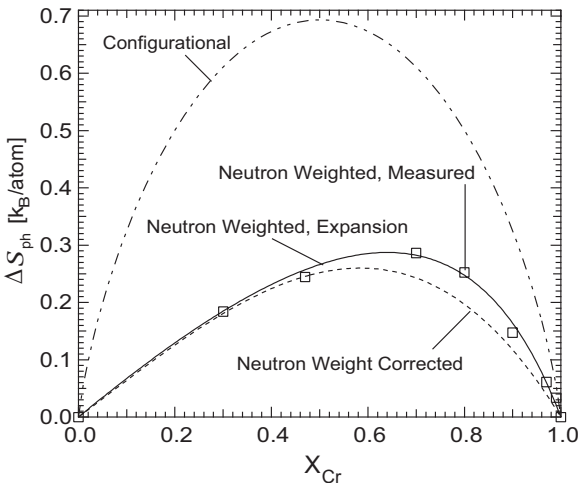

FIG. 10. Phonon entropy of mixing determined at 293 K for measured NWDOS curves (open squares), cluster expansion of measured NWDOS curves (solid line), and neutron-weight-corrected DOS curves (dashed line). The configurational entropy of a fully random solid solution is included to show the relative magnitude of the phonon entropy.

$$\Delta S_{\mathrm{ph}}(x_d, d) = -3k_B[1-(1-2x_d)^2] \int_0^\infty f^\star(E) \mathcal{G}_2(E,d) \mathrm{d}E. \tag{17}$$

The integrals of $3k_B f^\star(E)\mathcal{G}_n(E,d)$ are the interaction phonon partial entropies $s^n_{\mathrm{ph}}(d)$, which are listed in Table I for room temperature and 2000 K. Only the $n=0$ term has a strong dependence on $f^\star(E)$ so Eq. (17) is approximately independent of temperature. The magnitude of the phonon partial entropy of mixing of Cr is much larger than that of Fe. The function $f^\star(E)$ is largest at low energies so the differences between $s^2_{\mathrm{ph}}(\mathrm{Fe})$ and $s^2_{\mathrm{ph}}(\mathrm{Cr})$ can be primarily attributed to the low-energy modes from 0 to ~25 meV.

For a random solid solution, the phonon entropy of mixing of Eq. (15) is, in terms of the interaction phonon partial entropies,

$$\Delta S_{\mathrm{ph}}(x_{\mathrm{Cr}}) = -4x_{\mathrm{Cr}}(1-x_{\mathrm{Cr}})\{[s^1_{\mathrm{ph}}(\mathrm{Cr}) + s^1_{\mathrm{ph}}(\mathrm{Fe})]/2 + x_{\mathrm{Cr}} s^2_{\mathrm{ph}}(\mathrm{Cr}) + (1-x_{\mathrm{Cr}}) s^2_{\mathrm{ph}}(\mathrm{Fe})\}. \tag{18}$$

The function $-4x_{\mathrm{Cr}}(1-x_{\mathrm{Cr}})$ is a parabola with a maximum at $x_{\mathrm{Cr}}=1/2$. The first term in brackets scales this function. In this case, since $s^1_{\mathrm{ph}}(d)$ is negative, this term introduces a positive entropy of mixing. The remaining terms associated with

TABLE I. Values of $s^n_{\mathrm{ph}}(d)$.

	s^n_{ph}(Fe) [k_B/atom]		s^n_{ph}(Cr) [k_B/atom]	
n \ T[K]	293	2000	293	2000
0	3.20	8.83	3.14	8.76
1	−0.05	−0.05	−0.10	−0.11
2	−0.08	−0.11	−0.27	−0.29

$s^2_{\mathrm{ph}}(d)$, are the equation of a line. This function introduces an asymmetry to the phonon entropy of mixing when $s^2_{\mathrm{ph}}(\mathrm{Fe}) \neq s^2_{\mathrm{ph}}(\mathrm{Cr})$. The phonon entropy of mixing is shifted toward pure Cr because $\mathcal{G}_2(E,\mathrm{Cr}) < \mathcal{G}_2(E,\mathrm{Fe})$ in the energy range 0 to ~25 meV.

The critical temperature and composition of the miscibility gap in Fe-Cr are 905 K and $x_{\mathrm{Cr}}=0.51$, respectively.[52] Assuming no change in the DOS curves as a function of temperature, the values of $s^n_{\mathrm{ph}}(d)$ for $n>0$ do not appreciably change over the temperature range of bcc stability. Equation (18) can be used to determine the effect of the phonon entropy on the miscibility gap for spinodal decomposition. When the phonon entropy of mixing in the bcc phase is removed, the miscibility gap shifts up in temperature and toward pure Cr, with a critical temperature and composition of 1268 K and $x_{\mathrm{Cr}}=0.61$, respectively. It is known that the enthalpy of mixing is also shifted toward pure Cr,[53–56] so the phonon entropy counteracts the asymmetry of the enthalpy of mixing (especially at higher temperatures). Thus, the role of the phonon entropy of mixing is to lower the critical temperature of the miscibility gap and shift it toward the equiatomic composition.

The cluster expansion analysis delivers a higher level of detail about how the phonon entropy of mixing depends on local arrangements of atoms.[28] At low concentrations of Fe in a Cr host, there is a substantial distortion of the Fe PDOS curves compared to pure Fe, and there is a smaller distortion of the PDOS curves of Cr in Fe (Figs. 7 and 8). A comparison of $\mathcal{G}_1(\mathcal{E},\mathrm{Fe})$ and $\mathcal{G}_1(\mathcal{E},\mathrm{Cr})$ (Fig. 7) shows that the concentration dependence of the PDOS curves is opposite for the transverse modes but similar for the longitudinal modes. For Fe-Cr alloys, the PDOS curves of both Fe and Cr atoms undergo an average softening upon alloying. This leads to a net positive phonon entropy of mixing but the net softening of the Cr PDOS curves is greater. At low concentrations of Fe in Cr, the large softening of the Cr PDOS curves (compared to the Fe PDOS of dilute Cr in Fe) causes the phonon entropy of mixing to rapidly rise with Fe concentration, giving a skewness to the concentration dependence of the phonon entropy of mixing versus composition (Fig. 10). Changes in the shape of the PDOS of the majority species are relatively small yet most of the phonon thermodynamics of mixing can be attributed to the changes in the low-energy vibrations of the solvent species, especially Cr. It is expected that other alloy systems will have different entropic weights of their atom species, and these can be quantified by examining the IPDOS functions $\mathcal{G}_n(E,d)$.

V. CONCLUSION

Neutron-weighted phonon density of states (NWDOS) curves were measured by inelastic neutron scattering for Fe-Cr random solid solutions of various compositions. Within the formalism of the cluster expansion, the methods for extracting the interaction phonon density of states (IPDOS) functions from the NWDOS curves are described for random solid solutions (Appendixes A and B). From the cluster expansion analysis, phonon partial DOS (PDOS) curves were found for Fe and Cr in the different random solid solutions of Fe-Cr. The Fe PDOS curves are similar to those previously determined by NRIXS, and so are the Fe IPDOS functions.

Using Fe and Cr PDOS curves, it is straightforward to correct the inelastic neutron scattering from Fe-Cr alloys for the neutron weighting caused by differences in phonon scattering efficiencies of the two elements. The corrected DOS curves are stiffer than their neutron-weighted counterparts, owing to the higher scattering efficiency of the lower energy Fe modes and this lowers the phonon entropy of mixing that would otherwise be deduced from NWDOS curves obtained from a direct reduction in inelastic scattering data under the virtual crystal assumption.

The phonon entropy is dominated by changes in the Cr PDOS curves, which undergoes an average softening when Cr atoms are placed in an Fe-Cr host. The softening of the Cr PDOS curves is also responsible for the compositional asymmetry of the phonon entropy of mixing. The dominant effect on the phonon entropy is from changes in the low-energy modes of the Cr PDOS curves caused by 1NN and 2NN Fe neighbors. The phonon entropy both shifts the miscibility gap in composition toward the equiatomic composition and lowers the critical temperature by ~350 K.

ACKNOWLEDGMENTS

The authors are indebted to L. Jirik and K. Littrel for their technical support on the LRMECS instrument. This work has benefited from the use of the Intense Pulsed Neutron Source at Argonne National Laboratory. This facility is funded by the U.S. Department of Energy, BES-Materials Science, under Contract No. W-31-109-Eng-38. This work was supported by the U.S. Department of Energy through the Basic Energy Sciences Grant No. DE-FG02-03ER46055.

APPENDIX A: CLUSTER EXPANSION

The GCE is a method of expressing thermodynamic properties of an alloy in terms of its chemical arrangement $\vec{\sigma}$. "Spin variables" σ are used for the two species of atoms, where an A atom is assigned the factor $\sigma=+1$ and a B atom $\sigma=-1$. A cluster is a shape made by connecting a number of points n on the lattice. The correlation function ξ_n is defined as the sum over all clusters of the products of the spin variables for each atom in the cluster,

$$\xi_n = \frac{1}{N_n}\sum_{\{p_i\}} \sigma_{p_1}\sigma_{p_2}\cdots\sigma_{p_n}. \tag{A1}$$

Here, n also denotes the order of each term in the expansion. For example, in the GCE $n=\{0,1,2\}$ for the empty, point, and pair terms, respectively. The number of clusters of type n is N_n. The value of the spin variable at site p is σ_p with each lattice point labeled from 1 to n.[26] The correlation functions ξ_n for a random solid solution of A and B atoms are given by

$$\xi_n = (1-2x_B)^n. \tag{A2}$$

The Connolly-Williams inversion technique[26] can be applied to a thermodynamic quantity $J(\vec{\sigma})$. Interaction param-

eters of this thermodynamic quantity $\mathcal{J}_n$ can be determined using the known values of the thermodynamic quantity $J_m(\vec{\sigma})$,

$$\mathcal{J}_n = \sum_{m=0}^{\nu_g - 1} J_m(\vec{\sigma})[\xi_{m,n}]^{-1}. \tag{A3}$$

Here, ν_g is the number of terms used in the GCE and $[\xi_{m,n}]$ is the correlation function matrix. Knowledge of $\mathcal{J}_n$ can then be used to construct the thermodynamic quantity for any configuration $J_j(\vec{\sigma})$ by using

$$J_j(\vec{\sigma}) = \sum_{n=0}^{\nu_g - 1} \mathcal{J}_n[\xi_{j,n}]. \tag{A4}$$

The machinery of the previous two equations remains valid for functions by replacing $\mathcal{J}_n$ with $\mathcal{J}_n(E)$ and $J(\vec{\sigma})$ with $J(E,\vec{\sigma})$.

The LOCE is a method for expressing thermodynamic properties of a particular type of atom in terms of its local chemical arrangement σ_l. In the LOCE, the clusters must contain the local point of interest l (e.g., an A atom).[51] A cluster is a shape made by connecting a number of points $n+1$ on the lattice, where the +1 arises from the inclusion of the local point in all clusters. In the LOCE, $n=0$ is the point term because every point cluster is the atom of interest d, with $\sigma_l^d = +1$. The pair and triangle terms correspond to $n=1$ and $n=2$, respectively. The local point is always assigned $\sigma_l^d = +1$ so that for a binary system of A and B atoms two different correlation functions must be used. The correlation function for a random solid solution of A and B atoms around a local point containing an A atom is

$$\xi_n(A) = (1 - 2x_B)^n. \tag{A5}$$

For a local point containing a B atom the correlation function is

$$\xi_n(B) = (1 - 2x_A)^n = (-1)^n \xi_n(A). \tag{A6}$$

Again, the machinery of Eq. (A3) and Eq. (A4) remains valid for both quantities and functions in the LOCE. For functions in the LOCE, these equations are valid by replacing $\mathcal{J}_n$ with $\mathcal{J}_n(E,d)$, $J(\vec{\sigma})$ with $J(E,\vec{\sigma}_l,d)$, and ν_g with ν_l. Here, the dependence on d denotes a LOCE with a d atom as the atom at the local point of interest and ν_l is the number of terms used in the LOCE.

When the LOCE and GCE are both used to describe the same quantity, for example, the DOS and PDOS of Eq. (7), the number of terms used for each cluster expansion are related by $\nu_g = \nu_l + 1$. For instance, a three-term LOCE uses clusters up to the triangle term. The equivalent GCE must use four terms in the expansion to include the triangle term.

APPENDIX B: METHOD FOR DETERMINATION OF $\mathcal{G}_n(\mathcal{E},d)$

First, consider the basic problem for an A-B binary alloy using a four-term GCE, which requires 2×3 PDOS curves (2 atom species, three-term LOCE) to describe the four DOS curves. Figure 11 shows that the four measured DOS curves

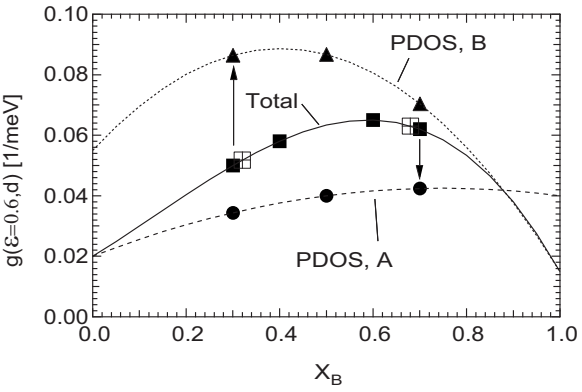

FIG. 11. Example of the cluster expansion method applied to the DOS and PDOS at a particular energy. See the text for a description of the symbols.

(black squares) used for the GCE (solid line) can never provide enough information to acquire the two PDOS curves (dashed lines). In other words, there must be information on at least one PDOS curve for each atom species in order to solve for the remaining PDOS curves from the measured DOS curves. However, by measuring two DOS curves of slightly different concentrations than the two end members (open squares with crosses), the difference method described in the text can be used to extract the minority species PDOS (indicated by arrows). In this manner, six measured DOS curves can be used to determine the six PDOS curves required to construct the IPDOS. In the remainder of this appendix, we describe the mathematics used to extract the IPDOS from the NWDOS.

The NWDOS curves of Eq. (8), $g_j^{\mathrm{nw}}(\mathcal{E},\vec{\sigma})$, can be written using Eq. (A4) in the LOCE formalism,

$$g_j^{\mathrm{nw}}(\mathcal{E},\vec{\sigma})\left\langle \frac{\sigma_{\mathrm{sc}}}{m} \right\rangle_d^{-1} = \sum_d x_{j,d} \frac{\sigma_{\mathrm{sc},d}}{m_d} g_j(\mathcal{E},\sigma_l,d), \tag{B1}$$

$$= \sum_d C_j(d) \sum_{n=0}^{\nu_l - 1} \mathcal{G}_n(\mathcal{E},d)[\xi_{j,n}(d)], \tag{B2}$$

$$= \sum_d C_j(d) \sum_{n=0}^{\nu_l - 1} [\xi_{j,n}(d)] \sum_{m=0}^{\nu_l - 1} g_m(\mathcal{E},\vec{\sigma}_l,d)[\xi_{m,n}(d)]^{-1}, \tag{B3}$$

where

$$C_j(d) = x_{j,d} \frac{\sigma_{\mathrm{sc},d}}{M_d}, \tag{B4}$$

$$A_j^{-1}(\vec{\sigma}) = \sum_d x_{j,d} \frac{\sigma_{\mathrm{sc},d}}{M_d}. \tag{B5}$$

Here, $g_j^{\mathrm{nw}}(\mathcal{E},\vec{\sigma})$ are the NWDOS curves constructed from the cluster expansion for each chemical arrangement $\vec{\sigma}$ corresponding to j. Similarly, $g_m(\mathcal{E},\vec{\sigma}_l,d)$ are the IPDOS curves for each chemical arrangement $\vec{\sigma}$ corresponding to m and are used to construct $\mathcal{G}_n(\mathcal{E},d)$. The concentrations of each atom species d corresponding to the chemical arrangement of j are

$x_{j,d}$. The NWDOS curves may also be written using Eq. (A4) in the GCE formalism,

$$g_j^{\mathrm{nw}}(\mathcal{E},\vec{\sigma})\left\langle \frac{\sigma_{\mathrm{sc}}}{m}\right\rangle_d^{-1} = \sum_{n=0}^{\nu_g-1} \mathcal{G}_n^{\mathrm{nw}}(\mathcal{E})[\xi_{j,n}], \tag{B6}$$

where $\mathcal{G}_n^{\mathrm{nw}}(\mathcal{E})$ are the NWIDOS functions.

Equations (B6) and (B2) can be used to relate $\mathcal{G}_n^{\mathrm{nw}}(\mathcal{E})$ to $\mathcal{G}_n(\mathcal{E},d)$:

$$\mathcal{G}_0^{\mathrm{nw}}(\mathcal{E}) = \frac{1}{2}\left[\frac{\sigma_{\mathrm{sc},A}}{m_A}\mathcal{G}_0(\mathcal{E},A) + \frac{\S c_{\mathrm{sc},B}}{m_B}\mathcal{G}_0(\mathcal{E},B)\right],$$

$$\mathcal{G}_n^{\mathrm{nw}}(\mathcal{E}) = \frac{1}{2}\left\{\frac{\sigma_{\mathrm{sc,A}}}{m_{\mathrm{A}}}[\mathcal{G}_{n-1}(\mathcal{E},A) + \mathcal{G}_n(\mathcal{E},A)] + (-1)^n\frac{\sigma_{\mathrm{sc},B}}{m_B}[\mathcal{G}_{n-1}(\mathcal{E},B) + \mathcal{G}_n(\mathcal{E},B)]\right\},$$

$$\mathcal{G}_{\nu_g-1}^{\mathrm{nw}}(\mathcal{E}) = \frac{1}{2}\left[\frac{\sigma_{\mathrm{sc},A}}{m_A}\mathcal{G}_{\nu_l-1}(\mathcal{E},A) + (-1)^n\frac{\sigma_{\mathrm{sc},B}}{m_B}\mathcal{G}_{\nu_l-1}(\mathcal{E},B)\right]. \tag{B7}$$

This can be written in matrix form as

$$\vec{\mathcal{G}}^{\mathrm{nw}}(\mathcal{E}) = ([R]\bullet[C])\vec{\mathcal{G}}_d(\mathcal{E}), \tag{B8}$$

where the • represents a Hadamard (element-wise) product and $[R]\bullet[C]$ is the matrix that relates the NWIDOS vector $\vec{\mathcal{G}}^{\mathrm{nw}}(\mathcal{E})$ with the IPDOS vector $\vec{\mathcal{G}}_d(\mathcal{E})$, which are defined as

$$\vec{\mathcal{G}}^{\mathrm{nw}}(\mathcal{E}) = \begin{Bmatrix} \mathcal{G}_0^{\mathrm{nw}}(\mathcal{E}) \\ \mathcal{G}_1^{\mathrm{nw}}(\mathcal{E}) \\ \vdots \\ \mathcal{G}_{\nu_g-1}^{\mathrm{nw}}(\mathcal{E}) \end{Bmatrix}, \quad \vec{\mathcal{G}}_d(\mathcal{E}) = \begin{Bmatrix} \mathcal{G}_0(\mathcal{E},\mathrm{A}) \\ \vdots \\ \mathcal{G}_{\nu_l-1}(\mathcal{E},\mathrm{A}) \\ \mathcal{G}_0(\mathcal{E},\mathrm{B}) \\ \vdots \\ \mathcal{G}_{\nu_l-1}(\mathcal{E},\mathrm{B}) \end{Bmatrix}. \tag{B9}$$

The elements of the $\nu_g \times 2\nu_l$ matrix $[C]$ of scattering coefficients are

$$C_{n\{j,d\}} = \frac{\sigma_{\mathrm{sc},d}}{m_d}, \tag{B10}$$

where $\{j,d\}$ is a compound index. For a three-term LOCE, the matrix $[R]$ is

$$[R] = 1/2\left[\begin{array}{ccc|ccc} 1 & 0 & 0 & 1 & 0 & 0 \\ 1 & 1 & 0 & -1 & -1 & 0 \\ 0 & 1 & 1 & 0 & 1 & 1 \\ 0 & 0 & 1 & 0 & 0 & -1 \end{array}\right], \tag{B11}$$

where the left half of the separation denotes the A atom type and the right half the B atom type. Note that the matrix $[R]$ relates the IDOS to the IPDOS functions,

$$\vec{\mathcal{G}}(\mathcal{E}) = [R]\vec{\mathcal{G}}_d(\mathcal{E}), \tag{B12}$$

which should be compared to Eq. (B8).

The NWIDOS, which are measured in the experiment, can now be written in terms of the PDOS as

$$\vec{\mathcal{G}}^{\mathrm{nw}}(\mathcal{E}) = ([R]\bullet[C])[\bar{\xi}]^{-1}\vec{g}_d(\mathcal{E}), \tag{B13}$$

where

$$\vec{g}_d(\mathcal{E}) = \begin{Bmatrix} g_0(\mathcal{E},A) \\ \vdots \\ g_{\nu_l-1}(\mathcal{E},A) \\ g_0(\mathcal{E},B) \\ \vdots \\ g_{\nu_l-1}(\mathcal{E},B) \end{Bmatrix}, \quad [\bar{\xi}] = \begin{bmatrix} [\xi_{m,n}(A)] & [0] \\ [0] & [\xi_{m,n}(B)] \end{bmatrix}. \tag{B14}$$

Here, $[\xi_{m,n}(d)]$ are the LOCE correlation function matrices corresponding to the PDOS curves $g_m(\mathcal{E},\sigma_l,d)$, which are written as the vector $\vec{g}_d(\mathcal{E})$. The PDOS of $\vec{g}_d(\mathcal{E})$ must be selected to include the PDOS determined from the difference method (or Mannheim method), which are termed the "known" PDOS curves $\vec{g}_k(\mathcal{E},d)$. The remaining or "unknown" PDOS curves $\vec{g}_u(\mathcal{E},d)$ can be solved for by row reducing the augmented matrix $[([R]\bullet[C])[\bar{\xi}]^{-1}\vec{\mathcal{G}}^{\mathrm{nw}}(\mathcal{E})]$ and rewriting the system of equations in parametric form.[57] The unknown PDOS curves can then be written as a function of the known PDOS curves and the NWIDOS functions,

$$\vec{g}_u(\mathcal{E},d) = [\mathcal{S}]\begin{Bmatrix} \vec{\mathcal{G}}^{\mathrm{nw}}(\mathcal{E}) \\ \vec{g}_k(\mathcal{E},d) \end{Bmatrix}, \tag{B15}$$

where $[\mathcal{S}]$ is the solution matrix and the term in brackets is an augmented column vector. Once $\vec{g}_u(\mathrm{E},d)$ has been determined, a direct inversion following:

$$\vec{\mathcal{G}}_d(\mathcal{E}) = [\bar{\xi}]^{-1}\vec{g}_d(\mathcal{E}), \tag{B16}$$

produces the IPDOS functions $\mathcal{G}_n(\mathcal{E},d)$.

[1] L. Anthony, J. K. Okamoto, and B. Fultz, Phys. Rev. Lett. **70**, 1128 (1993).
[2] A. van de Walle and G. Ceder, Rev. Mod. Phys. **74**, 11 (2002).
[3] P. D. Bogdanoff and B. Fultz, Philos. Mag. B **79**, 753 (1999).
[4] T. L. Swan-Wood, O. Delaire, and B. Fultz, Phys. Rev. B **72**, 024305 (2005).
[5] P. J. Craievich and J. M. Sanchez, Comput. Mater. Sci. **8**, 92 (1997).
[6] O. Delaire, T. Swan-Wood, and B. Fultz, Phys. Rev. Lett. **93**, 185704 (2004).

[7] G. Moraitis and F. Gautier, J. Phys. F: Met. Phys. **7**, 1421 (1977).
[8] M. E. Manley, R. J. McQueeney, B. Fultz, R. Osborn, G. H. Kwei, and P. D. Bogdanoff, Phys. Rev. B **65**, 144111 (2002).
[9] O. Delaire, M. Kresch, and B. Fultz, Philos. Mag. **85**, 3567 (2005).
[10] V. Ozoliņš, C. Wolverton, and A. Zunger, Phys. Rev. B **58**, R5897 (1998).
[11] V. Ozoliņš and M. Asta, Phys. Rev. Lett. **86**, 448 (2001).
[12] C. Wolverton and V. Ozoliņš, Phys. Rev. Lett. **86**, 5518 (2001).
[13] A. van de Walle, Z. Moser, and W. Gasior, Arch. Metall. **49**, 535 (2004).
[14] R. Arroyave, A. van de Walle, and Z.-K. Liu, Acta Mater. **54**, 473 (2006).
[15] S. K. Sinha and B. N. Harmon, Phys. Rev. Lett. **35**, 1515 (1975).
[16] C. M. Varma and W. Weber, Phys. Rev. B **19**, 6142 (1979).
[17] K.-M. Ho, C.-L. Fu, and B. N. Harmon, Phys. Rev. B **28**, 6687 (1983).
[18] O. Delaire and B. Fultz, Phys. Rev. Lett. **97**, 245701 (2006).
[19] M. H. F. Sluiter, M. Weinert, and Y. Kawazoe, Phys. Rev. B **59**, 4100 (1999).
[20] E. J. Wu, G. Ceder, and A. van de Walle, Phys. Rev. B **67**, 134103 (2003).
[21] J. Z. Liu, G. Ghosh, A. van de Walle, and M. Asta, Phys. Rev. B **75**, 104117 (2007).
[22] P. D. Bogdanoff, T. L. Swan-Wood, and B. Fultz, Phys. Rev. B **68**, 014301 (2003).
[23] P. D. Bogdanoff, B. Fultz, and S. Rosenkranz, Phys. Rev. B **60**, 3976 (1999).
[24] P. D. Bogdanoff and B. Fultz, Philos. Mag. B **81**, 299 (2001).
[25] A. F. Yue, A. Papandrew, P. D. Bogdanoff, I. Halevy, J. G.-W. Lin, B. Fultz, W. Sturhahn, E. E. Alp, and T. S. Toellner, Hyperfine Interact. **141-142**, 249 (2002).
[26] J. W. D. Connolly and A. R. Williams, Phys. Rev. B **27**, 5169 (1983).
[27] H. Y. Geng, M. H. F. Sluiter, and N. X. Chen, J. Chem. Phys. **122**, 214706 (2005).
[28] M. S. Lucas, A. Papandrew, B. Fultz, and M. Y. Hu, Phys. Rev. B **75**, 054307 (2007).
[29] T. J. Nichol, A. Datta, and G. Aggen, Metall. Trans. A **11A**, 573 (1980).
[30] K. L. Weng, H. R. Chen, and J. R. Yang, Mater. Sci. Eng., A **379**, 119 (2004).
[31] F. W. de Wette and A. Rahman, Phys. Rev. **176**, 784 (1968).
[32] V. F. Sears, E. C. Svensson, and B. M. Powell, Can. J. Phys. **73**, 726 (1995).
[33] M. Kresch, O. Delaire, R. Stevens, J. Y. Y. Lin, and B. Fultz, Phys. Rev. B **75**, 104301 (2007).
[34] D. Morgan, A. van de Walle, G. Ceder, J. D. Althoff, and D. de Fontaine, Modell. Simul. Mater. Sci. Eng. **8**, 295 (2000).
[35] E. E. Alp, W. Sturhahn, T. S. Toellner, J. Zhao, M. Hu, and D. E. Brown, Hyperfine Interact. **144-145**, 3 (2002).
[36] M. Seto, Y. Yoda, S. Kikuta, X. W. Zhang, and M. Ando, Phys. Rev. Lett. **74**, 3828 (1995).
[37] W. Sturhahn, T. S. Toellner, E. E. Alp, X. Zhang, M. Ando, Y. Yoda, S. Kikuta, M. Seto, C. W. Kimball, and B. Dabrowski, Phys. Rev. Lett. **74**, 3832 (1995).
[38] W. Sturhahn, Hyperfine Interact. **125**, 149 (2000).
[39] T. Ruckert, W. Keune, W. Sturhahn, M. Y. Hu, J. P. Sutter, T. S. Toellner, and E. E. Alp, Hyperfine Interact. **126**, 363 (2000).
[40] P. D. Mannheim, Phys. Rev. **165**, 1011 (1968).
[41] M. Seto, Y. Kobayashi, S. Kitao, R. Haruki, T. Mitsui, Y. Yoda, S. Nasu, and S. Kikuta, Phys. Rev. B **61**, 11420 (2000).
[42] B. Fultz, L. Anthony, J. L. Robertson, R. M. Nicklow, S. Spooner, and M. Mostoller, Phys. Rev. B **52**, 3280 (1995).
[43] D. G. Howard and R. H. Nussbaum, Phys. Rev. B **9**, 794 (1974).
[44] J. M. Sanchez and D. de Fontaine, *Structure and Bonding in Crystals* (Academic Press, New York, 1981), p. 117.
[45] J. M. Sanchez, F. Ducastelle, and D. Gratias, Physica A **128**, 334 (1984).
[46] F. Ducastelle, *Order and Phase Stability in Alloys* (North-Holland, Amsterdam, 1991), Chap. 4.
[47] A. Zunger, in *Statics and Dynamics of Alloy Phases*, edited by P. E. A. Turchi and A. Gonis (Plenum, New York, 1994), p. 361.
[48] R. Kikuchi, Phys. Rev. **81**, 988 (1951).
[49] D. de Fontaine, in *Solid State Physics*, edited by H. Ehrenreich, F. Seitz, and D. Turnbull (Academic, New York, 1979), Vol. 34, p. 73.
[50] D. de Fontaine, in *Solid State Physics*, edited by H. Ehrenreich and D. Turnbull (Academic, New York, 1994), Vol. 47, p. 33.
[51] D. Morgan, J. D. Althoff, and D. de Fontaine, J. Phase Equilib. **19**, 559 (1998).
[52] J.-O. Andersson and B. Sundman, CALPHAD: Comput. Coupling Phase Diagrams Thermochem. **11**, 83 (1987).
[53] T. Chart, F. Putland, and A. Dinsdale, CALPHAD: Comput. Coupling Phase Diagrams Thermochem. **4**, 27 (1980).
[54] A. Caro, M. Caro, E. M. Lapasso, and D. A. Crowson, Appl. Phys. Lett. **89**, 121902 (2006).
[55] P. Olsson, I. A. Abrikosov, L. Vitos, and J. Wallenius, J. Nucl. Mater. **321**, 84 (2003).
[56] E. G. Moroni and T. Jarlborg, Phys. Rev. B **47**, 3255 (1993).
[57] David C. Lay, *Linear Algebra and Its Applications* (Addison-Wesley, Reading, MA, 2003), Chap. 1.